EXTENSION OF THE LUGRE DYNAMIC TIRE FRICTION MODEL TO 2D MOTION

E. Velenis*, P. Tsiotras*, C. Canudas-de-Wit†

*School of Aerospace Engineering, Georgia Institute of Technology, Atlanta, GA 30332-0150, USA
tel:+1-404-894-9108 fax:+1-404-894-2760
e-mail:{efstathios_velenis,p.tsiotras}@ae.gatech.edu

†Laboratoire d' Automatique de Grenoble, MR CNRS 5528, ENSIEG-INPG, B.P.46
38 402 ST. Martin d' Heres, FRANCE
tel:+33-4-76826380 fax:+33-4-76826388
e-mail:canudas@lag.ensieg.inpg.fr

Keywords: 2D Dynamic Tire Friction Models.

Abstract

An extension of the LuGre dynamic friction model from longitudinal motion to longitudinal/lateral motion is developed. Applying this model to the motion of a tire we derive a model for tire-road contact forces and moments. A comparison of the steady-state behaviour of the dynamic model with existing static tire friction models is also presented. This comparison allows one to determine the values of the parameters for the new model. Introducing a set of mean states we reduce the order of the system and derive a model in lumped form which is useful for control purposes.

1 Introduction

In this paper we extend the longitudinal LuGre friction model for tire-road contact, presented in [1] and finalized in [2] and [3], to the longitudinal/lateral motion of a wheeled vehicle. Such an extension has also been attempted in [4] and [5]. In [4], the coupling of the forces in different directions was neglected, resulting into a set of two independent ode's describing the deflection of the bristles at the contact patch in longitudinal and lateral directions. In [5], the coupling of the forces in different directions was taken into consideration in accordance to an extension of a static friction model to longitudinal/lateral motion [6]. In [5], the anisotropy of the friction characteristics in steady-state, and the rotation of the wheel rim were neglected.

A more complete dynamic model was presented in [7], which took into consideration both the coupling of the friction forces in different directions and the anisotropy of the friction characteristics in steady-state, as well as the effects of the wheel rim rotation. The model in [7], however, is missing the major advantage of the LuGre model which is its lumped form. That is, a model using mean states along the contact patch described by one ode instead of a distributed model of infinite number of states or a discretized distributed model of a large number of states.

In this paper we extend the LuGre model taking into account all aspects neglected in [4] and [5] and, in addition, we derive a lumped model useful for control purposes. The extension given in this paper is based on physical properties of the friction forces such as dissipativity and at least local maximality of the dissipation rate [8].

In the first part of the paper we present a methodology that allows one to derive a static friction model for 2D motion. Using this methodology we derive a whole class of dynamic friction models. As a special case, we derive a LuGre friction model for 2D motion which reduces nicely to the longitudinal motion model in the 1D case. In the second part of the paper, using the same approach as in [1], [2] and [3], we derive a distributed tire friction model for the longitudinal/lateral motion of the tire. We also look at the steady-state behaviour of the new model and com-

pare it to the Pacejka tire model [6], to determine a set of realistic parameters for the former. Again, following the same approach as in the longitudinal motion model, we define a set of mean states and derive a reduced order lumped model. Finally, we include the effect of the wheel rim rotation to both the distributed and lumped models.

2 A Two-Dimensional Coulomb Friction Model

Recall the Coulomb friction model for longitudinal motion of a body, with linear velocity v. In this model the friction force coefficient is given by

$$\mu(v) = \begin{cases} \mu_k & \text{for } v > 0, \\ [-\mu_s, \mu_s] & \text{for } v = 0, \\ -\mu_k & \text{for } v < 0 \end{cases} \quad (1)$$

where μ_k is the kinetic and μ_s is the static friction coefficient. The friction force is $F = \mu F_n$ where F_n is the normal load. Typically, $\mu_s \geq \mu_k > 0$.
Consider now the case where $\mu_s = \mu_k$. We can derive the same model as in (1) by applying the Maximal Dissipation Rate Principle [8] to the following set of admissible friction coefficients

$$\mathcal{C} = \{\mu \in \mathbb{R} : |\mu_k^{-1}\mu| \leq 1\} \quad (2)$$

The friction force will be 'admissible' if it maximizes the dissipation rate, i.e.,

$$\mu^* = \text{argmax}_{\mu \in \mathcal{C}}(-\mu F_n v(t)), \quad \forall v, \forall t > 0 \quad (3)$$

It is easy to prove ([7], [8]) that the solution to (2), (3) is given by

$$\mu^* = -\text{sign}(v)\mu_k \quad (4)$$

Now consider the case of 2D motion. Let $M_k = \begin{bmatrix} \mu_{kx} & 0 \\ 0 & \mu_{ky} \end{bmatrix} > 0$ be the matrix of friction coefficients, with μ_{kx} and μ_{ky} the friction coefficients for longitudinal motion along the x and y directions respectively. The two coefficients could be the same for a completely symmetric situation but, in general, are different since friction characteristics change with the direction of motion.
The set of admissible coefficients is now defined as

$$\mathcal{C} = \{\mu \in \mathbb{R}^2 : \|M_k^{-1}\mu\| \leq 1\} \quad (5)$$

The friction force will again be 'admissible' if it maximizes the dissipation rate. Thus,

$$\mu^* = \text{argmax}_{\mu \in \mathcal{C}}(-F_n \mu^T v(t)), \quad \forall v, \forall t > 0 \quad (6)$$

The solution to (5), (6) is given by ([7], [8])

$$\mu^* = -\frac{M_k^2 v}{\|M_k v\|} \quad (7)$$

Observe that $\mu \in \mathcal{C}$ does not imply dissipativity of the friction force. Actually, $\mu \in \mathcal{C}$ implies $-\mu \in \mathcal{C}$ and if $F_n \mu^T v \geq 0$ then $-F_n \mu^T v \leq 0$. On the other hand, conditions (2), (3) or (5), (6) together imply dissipativity of the friction force. Since $0 \in \mathcal{C}$, it follows that $F_n \mu^{*T} v \leq 0$. The set $\mathcal{C}$ provides bounds for the friction forces and also a coupling between the forces in different directions (Fig. 1). Finally, observe that the maximization of the dissipation rate was done for the case where $v \neq 0$. Obviously when $v = 0$ the dissipation rate $D(v) = 0$. In this case the friction coefficient is bounded by the static friction coefficients $\mu^* \in [-\mu_s, \mu_s]$.

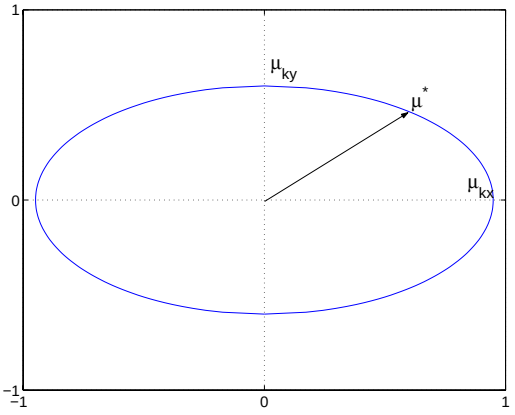

Figure 1: Set $\mathcal{C}$ of admissible coefficients for the 2D Coulomb case

3 A Class of Two-Dimensional Dynamic Friction Models

Using a set $\mathcal{C}$ of admissible friction coefficients and the Maximal Dissipation Rate Principle, a similar approach is followed in [7] and [8] in order to derive dynamic friction models for the 2D motion of a body. Let $M_k = \begin{bmatrix} \mu_{kx} & 0 \\ 0 & \mu_{ky} \end{bmatrix} > 0$ be the

matrix of asymptotic friction coefficients and $K = F_n \begin{bmatrix} \sigma_{0x} & 0 \\ 0 & \sigma_{0y} \end{bmatrix} > 0$ be the matrix of transient stiffnesses. Denote by u the relative deformation of the contact area of the body and by $F_D = \mu_D F_n$ the associated stress. Consider the elastic and plastic deformations $u_e = F_n K^{-1} \mu_D$ and $u_p = u - u_e$ respectively. Then, $D(\dot{u}_p) = -F_n \mu_D^T \dot{u}_p$ is the dissipation rate that must be positive and maximal.

In the case of dynamic friction models, the maximization of the dissipation rate is done locally, with respect to a neighborhood of each friction force candidate. The friction coefficient μ^* is given by the following Quasi Variational Inequality

$$\begin{aligned} -(\dot{u} - F_n K^{-1} \dot{\mu^*})^T (\mu^* - \mu) \geq 0 \\ \forall \mu \in \mathcal{C} = \{\mu \in \mathbb{R}^2 : \|M_k^{-1} \mu\| \leq \|M_k^{-1} \mu^*\|\} \end{aligned} \quad (8)$$

The above QVI has many solutions. In [7] and [8] a class of solutions is proposed generating a class of dynamic friction models. It is proven in [7], [8] that any solution μ^* of

$$-F_n K^{-1} \dot{\mu^*} - \lambda(u, \dot{u}, \mu^*) M_k^{-2} \mu^* = \dot{u} \quad (9)$$

where $\mu^*(0) = \mu_0$, satisfies (8) for all $\lambda(u, \dot{u}, \mu^*) \geq 0$. Several multi-dimensional dynamic friction models can be derived using (9) by choosing different scalar functions $\lambda(u, \dot{u}, \mu^*)$. The LuGre model is given for

$$\lambda(u, \dot{u}, \mu^*) = \lambda(\dot{u}) = \frac{\|M_k^2 \dot{u}\|}{g(\dot{u})} \quad (10)$$

with

$$g(\dot{u}) = \frac{\|M_k^2 \dot{u}\|}{\|M_k \dot{u}\|} + \tilde{g}(\|M_k \dot{u}\|) \quad (11)$$

where $\tilde{g}(\|M_k \dot{u}\|) \to 0$ when $\dot{u} \to +\infty$. Note that we wish to derive a model which asymptotically (as $\dot{u} \to +\infty$) approaches the Coulomb model (7) presented in the previous section. Notice that the function $g(\dot{u})$ characterizes the steady-state (static portion) of our dynamic model. This justifies the choice of the particular $\lambda(u, \dot{u}, \mu^*)$ in (10).

4 LuGre Friction Model for 2D Motion

The LuGre type friction model proposed in the previous section assumes that the friction is proportional only to the deflection of the bristles at the contact point z. In fact, it is assumed that $\mu = -(K/F_n)z$ and thus $\dot{\mu} = -(K/F_n)\dot{z}$. In order to include the dependence of the friction on the rate of z and the relative velocity at the point of contact $\dot{u}$, we rewrite equation (9) in terms of the internal friction state z. We then have [9]

$$\dot{z} = \dot{u} - \lambda(u, \dot{u}, z) M_k^{-2} \frac{K}{F_n} z \quad (12)$$

Recall that the function $\lambda(u, \dot{u}, z)$ proposed for the LuGre model is given in (10). Finally, we choose $g(\dot{u})$ and $\tilde{g}(\dot{u})$ to be able to recover the LuGre friction model of [9] for longitudinal motion. To this end, we choose

$$g(\dot{u}) = \frac{\|M_k^2 \dot{u}\|}{\|M_k \dot{u}\|} + \left(\frac{\|M_s^2 \dot{u}\|}{\|M_s \dot{u}\|} - \frac{\|M_k^2 \dot{u}\|}{\|M_k \dot{u}\|} \right) e^{\left(\frac{\|\dot{u}\|}{v_s}\right)^\alpha} \quad (13)$$

where $M_s = \begin{bmatrix} \mu_{sx} & 0 \\ 0 & \mu_{sy} \end{bmatrix}$ is the matrix of static friction coefficients. Finally, the friction coefficient vector is given by

$$\begin{aligned} \mu &= -\begin{bmatrix} \sigma_{0x} & 0 \\ 0 & \sigma_{0y} \end{bmatrix} z - \begin{bmatrix} \sigma_{1x} & 0 \\ 0 & \sigma_{1y} \end{bmatrix} \dot{z} \\ &\quad - \begin{bmatrix} \sigma_{2x} & 0 \\ 0 & \sigma_{2y} \end{bmatrix} \dot{u} \end{aligned} \quad (14)$$

Equations (10),(12), (13) and (14) represent the LuGre friction model for longitudinal/lateral motion of a body. The model reduces nicely to the longitudinal motion model of [9] in the 1D case.

The equations above are written in vector form. We next rewrite the equations in terms of the x and y components. Let $z = \begin{bmatrix} z_x \\ z_y \end{bmatrix}$, $\mu = \begin{bmatrix} \mu_x \\ \mu_y \end{bmatrix}$ and $\dot{u} = v_r = \begin{bmatrix} v_{rx} \\ v_{ry} \end{bmatrix}$. The friction model is then written as follows

$$\begin{aligned} \dot{z}_i &= v_{ri} - C_{0i}(v_r) z_i \\ \mu_i &= -\sigma_{0i} z_i - \sigma_{1i} \dot{z}_i - \sigma_{2i} v_{ri} \end{aligned} \quad (15)$$

where

$$C_{0i}(v_r) = \frac{\lambda(v_r) \sigma_{0i}}{\mu_{ki}^2}, \quad i = x, y \quad (16)$$

The scalar function $\lambda(v_r)$ is given by (10) and the function $g(v_r)$ by (13). Observe that the forces in the

x and y directions are coupled which is consistent with the property of the two-dimensional Coulomb friction model (7) presented earlier in the paper. The coupling term is $\lambda(v_r)$.

5 Two-Dimensional LuGre Tire Friction Model

5.1 Distributed Model

In this section we apply the LuGre friction model for 2D motion, to the motion of a tire in order to derive a model for tire-road contact forces and moments. We follow an approach similar to that in [1] and [3]. We assume that the contact patch of the tire, at the area of contact with the road, is a rectangular area (Fig. 2), divided into infinitesimal elements. For each element we apply the point LuGre model for 2D motion. In order to find the total forces and moments we integrate the forces of each element along the patch. To this end, let v denote the velocity of

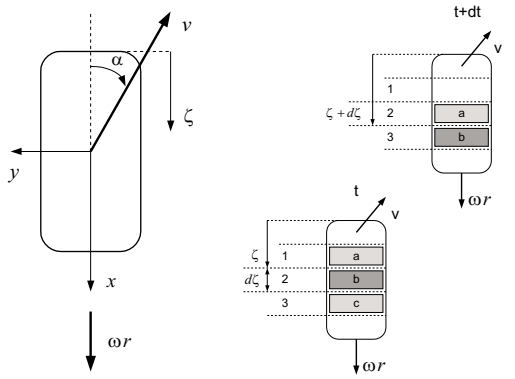

Figure 2: Frames of reference and velocities at the contact patch

the vehicle and ω the angular velocity of the wheel. The wheel has radius r. Let α be the angle of slip of the wheel, that is, the angle between the velocity vector and the x (longitudinal) body axis of the tire. Let us also assume for the time being, that the wheel rim is not rotating, i.e., the steering angle is constant. The relative velocity components of the wheel with respect to the ground are

$$v_{rx} = \omega r - v\cos(\alpha) \quad (17a)$$
$$v_{ry} = -v\sin(\alpha) \quad (17b)$$

In general, the velocity of the tire has components in both x and y axes with respect to the inertial frame. Considering a frame fixed on the contact patch, we observe that the tire elements move only along the length of the patch (ζ direction). For each tire element on the patch we can compute the friction using the LuGre model of the previous section. If we look at a fixed area on the patch then the internal friction states z_i become functions of both t and ζ.
Let $z_i(t,\zeta)$ denote the deflections of the patch element along x and y directions located at the point ζ along the patch at a certain time t (element b in Fig. 2). Consider the total deflections of this element between two time instances t and $t+dt$. Since the time interval dt the element has moved to the location $\zeta + d\zeta$, and using (15) we have that the total deflection dz is

$$\begin{aligned} dz_i &= z_i(t+dt,\zeta+d\zeta) - z_i(t,\zeta) \\ &= (v_{ri} - C_{0i}(v_r)z_i(t,\zeta))dt, \;\; i = x,y \end{aligned}$$

Since $dz = \frac{\partial z}{\partial \zeta}d\zeta + \frac{\partial z}{\partial t}dt$ and using the fact that $d\zeta/dt = |\omega r|$ the friction model is summarized by the following equations

$$\begin{aligned} \frac{dz_i(t,\zeta)}{dt} &= \frac{\partial z_i(t,\zeta)}{\partial t} + \frac{\partial z_i(t,\zeta)}{\partial \zeta}|\omega r| \\ &= v_{ri} - C_{0i}(v_r)z_i \\ \mu_i(t,\zeta) &= -\sigma_{0i}z_i(t,\zeta) - \sigma_{1i}\frac{\partial z_i(t,\zeta)}{\partial t} \\ &- \sigma_{2i}v_{ri}, \end{aligned} \quad (18)$$

where $i = x, y$. The total forces along the x and y directions are

$$F_i(t) = \int_0^L \mu_i(t,\zeta)f_n(\zeta)d\zeta, \quad i = x,y \quad (19)$$

where $f_n(\zeta)$ is the normal load distribution along the contact patch. The force distribution along the y direction results into a moment about the center of the patch (aligning torque) given by

$$M_z(t) = -\int_0^L \mu_y(t,\zeta)f_n(\zeta)\left(\frac{L}{2} - \zeta\right)d\zeta \quad (20)$$

Next, we evaluate our distributed model by comparing it to other tire models. In particular, we compare it to Pacejka's Magic Formula [6] which is widely

used in the automotive industry and captures reality accurately under steady-state conditions (i.e., for constant vehicle speed and wheel angular speed). In what follows, we examine the forces predicted by our distributed model under such steady-state conditions.

5.2 Steady-State Conditions

As seen in [1], [2] and [3] the steady-state time characteristics of the model (18) are obtained by setting $\frac{\partial z(t,\zeta)}{\partial t} = 0$, and imposing that the velocities v and ω are constant. In this case, the pde in (18) becomes

$$\frac{\partial z_i(t,\zeta)}{\partial \zeta} = \frac{1}{|\omega r|}\left(v_{ri} - C_{0i}(v_r) z_i\right), \quad i = x, y$$

Enforcing the boundary condition $z(t,0) = 0$ and the steady-state conditions of constant v and ω we integrate (21) to obtain

$$z_i^{ss}(\zeta) = C_{1i}\left(1 - e^{-\frac{\zeta}{C_{2i}}}\right), \quad i = x, y \tag{21}$$

where

$$C_{1i} = \frac{v_{ri}\mu_{ki}^2}{\lambda(v_r)\sigma_{0i}}, \quad C_{2i} = \frac{|\omega r|}{C_{0i}}, \quad i = x, y \tag{22}$$

We can now compute the steady-state expressions for the forces and the alignment torque using (19) and (20). In particular, we have

$$F_i^{ss} = -\int_0^L \left(\sigma_{0i} z_i^{ss} + \sigma_{2i} v_{ri}\right) f_n(\zeta) d\zeta \tag{23}$$

$$M_z^{ss} = \int_0^L \left(\sigma_{0y} z_y^{ss} + \sigma_{2y} v_{ry}\right) f_n(\zeta) \left(\frac{L}{2} - \zeta\right) d\zeta \tag{24}$$

where $i = x, y$. Before we proceed with the calculations, a few words about the normal load distribution f_n are in order. We are tempted to assume uniform load distribution i.e. $f_n = \text{const}$. This is not a realistic assumption, because the uniform load distribution does not satisfy the natural boundary conditions of zero normal load at the edges of the patch. In addition, the uniform load distribution would lead to an aligning torque that is not changing sign for higher lateral slip angles as observed in practice. To this end, we adopt a more realistic but still quite simple to integrate load distribution, namely, the trapezoidal distribution, as proposed by Deur et. al. in [5]. In this case, the function f_n is given by

$$f_n(\zeta) = \begin{cases} \alpha_1 \zeta & \text{for } 0 \le \zeta \le \zeta_L, \\ f_{\max} & \text{for } \zeta_L \le \zeta \le \zeta_R, \\ \alpha_2 \zeta + \beta_2 & \text{for } \zeta_R \le \zeta \le L \end{cases} \tag{25}$$

with $f_{\max}$ the maximum value of the normal load distribution. ζ_L and ζ_R are parameters which determine where the distribution is linear and where it is constant, and

$$\alpha_1 = \frac{f_{\max}}{\zeta_L}, \;\; \alpha_2 = -\frac{f_{\max}}{L - \zeta_R}, \;\; \beta_2 = \frac{L f_{\max}}{L - \zeta_R} \tag{26}$$

The normal force on the wheel shaft is therefore,

$$F_n = \int_0^L f_n(\zeta) d\zeta = \frac{L + \zeta_R - \zeta_L}{2} f_{\max} \tag{27}$$

This normal load distribution (Fig. 3), is certainly closer to reality and satisfies the natural boundary conditions. It finally allows one to tune the point where the total forces act, thus overcoming the problem of the aligning torque sign reversal. Next, we calculate the expressions (23) and (24). Using the definitions of longitudinal slip, for the braking and accelerating cases [4]

$$s = \begin{cases} \dfrac{v_{rx}}{\omega r} & \text{for } v\cos(\alpha) < \omega r, \\ -\dfrac{v_{rx}}{v\cos(\alpha)} & \text{for } \omega r \le v\cos(\alpha) \end{cases} \tag{28}$$

we construct the steady-state $s - F_x, F_y$ and $\alpha - M_z$ plots (Fig. 4). Observe that they have the desired shape when compared to Pacejka's Magic Formula [6].

5.3 Parameter Fitting

In this section, and in order to obtain a set of realistic parameters for our tire model, we compare the steady-state expressions derived in the previous section with the Pacejka tire model [6]. The Pacejka model consists of a mathematical formula (the so called 'magic' formula) with parameters chosen to fit experimental data. The same formula, with different sets of parameters, can be used to generate the

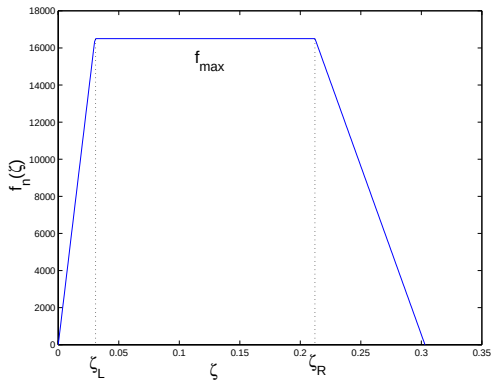

Figure 3: Trapezoidal Load Distribution

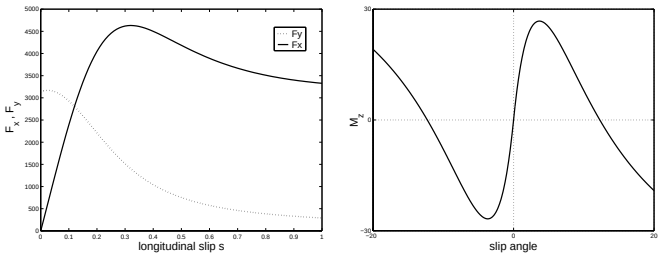

Figure 4: Steady-State Forces and Aligning Moment

plots of the longitudinal friction force F_x vs longitudinal slip s, the lateral friction force F_y vs slip angle α and the aligning torque M_z vs slip angle. Pacejka's formula is as follows

$$\begin{aligned} Y &= D\sin(\mathrm{Carctan}(\mathrm{B}\phi)) \\ \text{with } \phi &= (1-E)X + (E/B)\arctan(\mathrm{BX}) \end{aligned}$$

where X is either s or α and Y being F_x, F_y or M_z. We have chosen three sets of parameters B, C, D and E for the three different plots taken from [6]. The F_x plot is for pure braking i.e., longitudinal motion with $\alpha = 0$ and vehicle speed 60 km/h. The F_y and M_z plots are for pure cornering i.e., $s = 0$ and vehicle speed 70 km/h. In all cases the normal load was $F_n = 2000$Nt. The parameters for the three plots are given in the following table. The identification of the

Table 1: Pacejka Parameters

Parameters	B	C	D	E
F_x	0.178	1.55	2193	0.432
F_y	0.244	1.5	1936	-0.132
M_z	0.247	2.56	-15.53	-3.92

LuGre tire model parameters was done by fitting the plots generated by the steady-states (23) and (24) to the Pacejka plots using the parameters above. The identified parameters are given in the following table and the results of the curve fitting are shown in Fig. 5.

Table 2: Identified Parameters

$\sigma_{0x}(1/\mathrm{m})$	μ_{kx}	μ_{sx}	$\sigma_{2x,y}(\mathrm{sec/m})$
247	0.75	1.24	0
$\sigma_{0y}(1/\mathrm{m})$	μ_{ky}	μ_{sy}	α
211	0.79	1.18	1
$L(\mathrm{m})$	r_l	r_r	$v_s(\mathrm{m/sec})$
0.3	0.4	0.47	4.02

5.4 Average Lumped Model

Recall the expression for the total forces on the contact patch. According to (19) we have

$$F_i(t) = -\int_0^L \left(\sigma_{0i} z_i + \sigma_{1i}\frac{\partial z_i}{\partial t} + \sigma_{2i} v_{ri}\right) f_n(\zeta) d\zeta$$

where $i = x, y$. Define now, as in [3], the mean internal friction state $\bar{z}$ as follows

$$\bar{z}_i(t) = \frac{1}{F_n}\int_0^L z_i(t,\zeta) f_n(\zeta) d\zeta, \quad i = x, y \qquad (29)$$

and thus we also have

$$\frac{d\bar{z}_i(t)}{dt} = \frac{1}{F_n}\int_0^L \frac{\partial z_i(t,\zeta)}{\partial t} f_n(\zeta) d\zeta, \quad i = x, y \qquad (30)$$

The total friction force can then be written in terms of the mean state $\bar{z}$ as follows,

$$F_i(t) = -F_n\left(\sigma_{0i}\bar{z}_i(t) + \sigma_{1i}\dot{\bar{z}}_i(t) + \sigma_{2i} v_{ri}\right) \qquad (31)$$

Finally, we need to find the dynamics of the mean state. To this end, from (29) we have

$$\begin{aligned} \dot{\bar{z}}_i(t) &= \frac{1}{F_n}\int_0^L \left(v_{ri} - C_{0i}(v_r) z_i - \frac{\partial z_i}{\partial \zeta}|\omega r|\right) f_n d\zeta \\ &= v_{ri} - C_{0i}(v_r)\bar{z}_i - \frac{|\omega r|}{F_n}[z_i(t,\zeta) f_n(\zeta)]_0^L \\ &+ \frac{|\omega r|}{F_n}\int_0^L z_i \frac{\partial f_n}{\partial \zeta} d\zeta \\ &= v_{ri} - C_{0i}(v_r)\bar{z}_i - \kappa_i(t)|\omega r|\bar{z}_i, \quad i = x, y \end{aligned} \qquad (32)$$

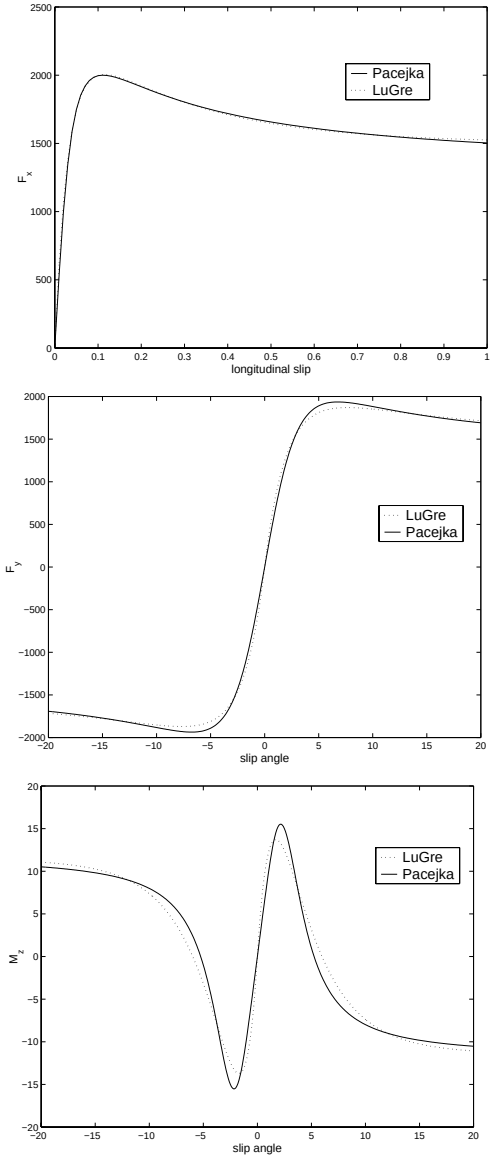

Figure 5: LuGre - Pacejka comparison

where,

$$\kappa_i(t) = -\frac{\int_0^L z_i \frac{\partial f_n}{\partial \zeta} d\zeta}{\int_0^L z_i f_n d\zeta}, \quad i = x, y \tag{33}$$

Obviously $(|\omega r|/F_n)[z_i(t,\zeta) f_n(\zeta)]_0^L = 0$ because of the assumed normal load distribution in (25).
The $\kappa_i(t)$ term in (33) was introduced in order to write the last term of the equation (32) in terms of the mean state $\bar{z}_i$. The $\kappa_i(t)$ term is difficult to compute using (33). To this end, we choose to approximate $\kappa_i(t)$ in a way that the steady-state solution of the lumped model is the same with the one of the distributed model, as it was done in [2] and [5]. The steady-state of the lumped model is found by setting $\dot{\bar{z}}_i(t) = 0$. Hence,

$$\bar{z}_i^{ss} = \frac{v_{ri}}{C_{0i}(v_r) + \kappa_i |\omega r|}, \quad i = x, y \tag{34}$$

In order for the distributed and the lumped models to produce the same steady-state forces, we enforce $F_i^{ss} \equiv \bar{F}_i^{ss}$, which implies $z_i^{ss} \equiv \bar{z}_i^{ss}$. Solving for κ_i we get that

$$\kappa_i = \frac{1}{|\omega r|} \left(\frac{v_{ri}}{z_i^{ss}} - C_{0i} \right), \quad i = x, y \tag{35}$$

where z_i^{ss} is given by (21).
Next, recall the expression for the total aligning torque along the contact patch

$$\begin{aligned} M_z(t) = {} & \frac{L}{2} \left(\sigma_{0y} \bar{z}_y(t) + \sigma_{1y} \dot{\bar{z}}_y(t) + \sigma_{2y} v_{ry} \right) - \\ & - \sigma_{0y} \int_0^L z_y f_n \zeta d\zeta + \sigma_{1y} \int_0^L \frac{\partial z_y}{\partial t} f_n \zeta d\zeta \\ & + \sigma_{2y} v_{ry} \int_0^L f_n \zeta d\zeta \end{aligned} \tag{36}$$

and define the mean internal state $\hat{z}_y$ as follows

$$\hat{z}_y(t) = \frac{1}{F_n L} \int_0^L z_y(t,\zeta) f_n(\zeta) \zeta d\zeta \tag{37}$$

Thus,

$$\frac{d\hat{z}_y(t)}{dt} = \frac{1}{F_n L} \int_0^L \frac{\partial z_y(t,\zeta)}{\partial t} f_n(\zeta) \zeta d\zeta \tag{38}$$

The total aligning torque can then be written in terms of the mean states $\bar{z}_y$ and $\hat{z}_y$, as follows

$$\begin{aligned} \frac{M_z(t)}{F_n L} = {} & \sigma_{0y} \left(\frac{1}{2} \bar{z}_y(t) - \hat{z}_y(t) \right) \\ & + \sigma_{1y} \left(\frac{1}{2} \dot{\bar{z}}_y(t) - \dot{\hat{z}}_y(t) \right) + \sigma_{2y} \left(\frac{1}{2} v_{ry} - \frac{\eta}{F_n L} \right) \end{aligned}$$

where,

$$\begin{aligned} \eta = {} & \int_0^L f_n(\zeta) \zeta d\zeta \\ = {} & \frac{\alpha_1}{3} \zeta_L^3 + \frac{f_{max}}{2} \left(\zeta_R^2 - \zeta_L^2 \right) \\ & + \frac{\alpha_2}{3} \left(L^3 - \zeta_R^3 \right) + \frac{\beta}{2} \left(L^2 - \zeta_R^2 \right) \end{aligned} \tag{39}$$

in case of a trapezoidal normal load distribution as in (25). Finally, we need to find the dynamics of the mean state. Using (37) we have that

$$\dot{\bar{z}}_y(t) = \frac{1}{F_n L}\int_0^L \frac{\partial z_y}{\partial t} f_n \zeta d\zeta = \frac{\eta}{F_n L} v_{ry} - C_{0y}(v_r)\bar{z}_y - \hat{\kappa}(t)|\omega r|\bar{z}_y + \frac{|\omega r|}{L}\bar{z}_y \quad (40)$$

where,

$$\hat{\kappa}(t) = -\frac{\int_0^L z_y \frac{\partial f_n}{\partial \zeta}\zeta d\zeta}{\int_0^L z_y f_n \zeta d\zeta} \quad (41)$$

Obviously $(|\omega r|/(F_n L))[z_i(t,\zeta) f_n(\zeta)\zeta]_0^L = 0$ because of the assumption for the normal load distribution in (25).

Following the same reasoning as in the case of the lumped model forces, we compute the $\hat{\kappa}$ term by requiring that the steady-state aligning torque predicted by the lumped model $\hat{M}_z^{ss}$ is the same with the one predicted by the distributed model M_z^{ss}. The steady-state of the lumped model is found for $\dot{\bar{z}}_y = 0, \bar{z}_y = 0$. This requirement leads to the desirable steady-state of $\bar{z}_y$, as follows

$$\bar{z}_y^{ss} = \frac{1}{2\sigma_{0y}}(\sigma_{0y}\bar{z}_y + \sigma_2 v_{ry}) - \frac{M_z^{ss}}{F_n L \sigma_{0y}} - \frac{\eta \sigma_2 v_{ry}}{\sigma_{0y}}$$

To compute $\hat{\kappa}$ we set $\dot{\bar{z}}_y = 0$ in (40). We then have

$$\hat{\kappa} = \frac{1}{|\omega r|}\left(\frac{1}{\hat{z}_{SSy}}\left(\frac{\eta v_{ry}}{F_n L} + \frac{|\omega r|\bar{z}_y^{ss}}{L}\right) - C_{0y}\right) \quad (42)$$

where $\bar{z}_y^{ss}$ from (34).

5.5 Rotation of the wheel rim

So far, we have derived a model that predicts the friction forces and moments at the contact patch of the wheel when there is some lateral slip α, but the steering angle of the wheel ϕ remains constant. In order to include the effect of the angular velocity of the wheel rim, we first need to rewrite the expression for the relative velocity at the contact patch. We thus have

$$v_{rx} = \omega r - v\cos(\alpha) \quad (43a)$$

$$v_{ry}(\zeta) = -v\sin(\alpha) - \left(\frac{L}{2} - \zeta\right)\dot{\phi} \quad (43b)$$

Observe that in this case the relative velocity v_{ry} is a function of the position on the contact patch ζ. This does not affect the way we compute the forces and moments using the distributed model (18)-(20). However, there is a problem with the lumped model. Since v_{ry} depends on ζ we cannot use definition (29) and the approach of (32) to reduce the distributed model to a lumped form, because the term $C_{0i}(v_r)$ depends on ζ.

At this point, let us consider the torsional deflection of the contact patch, not as a result of the lateral force distribution along with torsional deflection of the bristles as was done in [7], but as a result of the lateral force distribution only. That is, we consider the total moment about vertical axis to have two components. One (M_z) is due to the lateral forces in the presence of some lateral slip α and it is computed by (39) and (40), considering (17b) as the definition of the relative velocity. The second component (M_{z-tor}) is due to the torsional deflection of the contact patch in the presence of wheel rim rotation. Since this component is not the result of torsional deflection of the bristles, a lumped model is sufficient to describe the dynamics of this part of the moment. We assume that the dynamics of this component have the general form of the LuGre friction model. We thus postulate

$$\dot{z}_z(t) = \dot{\phi} - \frac{\sigma_{0z}|\dot{\phi}|}{g_z(\dot{\phi})} z_z(t) \quad (44)$$

$$g_z(\dot{\phi}) = \mu_{kz} + (\mu_{sz} - \mu_{kz})\, e^{-\left(\frac{\dot{\phi}}{\dot{\phi}_s}\right)^{\beta}} \quad (45)$$

$$M_{z-tor} = -F_n L\left(\sigma_{0z} z_z + \sigma_{1z}\dot{z}_z + \sigma_{2z}\dot{\phi}\right) \quad (46)$$

The total moment predicted by the lumped model will then be the summation of M_{z-tor} and the component given by (39) considering (17)

$$M_{z-total} = M_z + M_{z-tor} \quad (47)$$

There is one final point that needs to be clarified. It is not only the aligning torque that needs adjustment when we include the effects of the wheel rim rotation. Since the expression of v_{ry} is changing, there should be some adjustment for the lateral forces as

well. To simplify the model, we assume that the rotation of the rim does not affect the friction forces and that the definition (17) can be used for the relative velocity. This is a realistic assumption, since in relatively high speeds the term $\left(\frac{L}{2}-\zeta\right)\dot{\phi}$ is much smaller compared to $v\sin(\alpha)$ due to the small length of the patch and the relatively small steering velocity $\dot{\phi}$. In smaller vehicle velocities the above might not be true, but in this case the normal load distribution is closer to a uniform one, resulting in cancellation of the lateral forces due to wheel rim rotation.

Concluding, we emphasize that the introduction of equations (44)-(46) was done artificially, because the total forces and moments were computed considering only the longitudinal and lateral deflection of the bristles. In other words, the coefficients of (44)-(46) are related to the friction characteristics of the distributed model. Next, we propose a steady-state scenario ($v=0$, $\omega=0$ and $\dot{\phi}\neq 0$) in order to predict the aligning torque of the distributed model, and then identify the remaining coefficients in a way such that the behavior of the lumped model captures the behavior of the distributed one at steady-state.

5.6 Identification of the Torsional Equation Parameters

In this section we identify the parameters of the torsional equations (44)-(46) of the average lumped model by comparing it with the distributed model using a special steady-state case scenario.

In particular, consider the case where $\omega, v=0$ and $\dot{\phi}=\text{const}$. The relative velocity v_r is then

$$\begin{aligned} v_{rx} &= 0 \\ v_{ry} &= -\dot{\phi}\left(\frac{L}{2}-\zeta\right) \end{aligned} \tag{48}$$

In this particular case, and since $\omega=0$, the equations of the internal friction states become

$$\frac{\partial z_i}{\partial t}+\frac{\partial z_i}{\partial \zeta}|\omega r| = \frac{\partial z_i}{\partial t} = v_{ri}-C_{0i}(v_r)z_i \tag{49}$$

where $i=x,y$. Also, in steady-state, we have $\frac{\partial z_i}{\partial t}=0$ which leads to the following value for the steady-state internal friction state

$$z_i^{ss}=\frac{v_{ri}}{C_{0i}(v_r)}, \qquad i=x,y \tag{50}$$

Obviously, and since $v_{rx}=0$, we have $z_x^{ss}=0$ and the steady-state longitudinal force is $F_x^{ss}=0$.

As far as the value of z_y^{ss} is concerned, we have

$$z_y^{ss}=\text{sign}(v_{ry})\frac{g(v_r)}{\sigma_{0y}} \tag{51}$$

Now observe that for $v_{rx}=0$ and $\alpha=1$ (as identified in a previous section) the function $g(v_r)$ becomes

$$g=\mu_{ky}+(\mu_{sy}-\mu_{ky})e^{-\frac{\mu_{ky}|\dot{\phi}|L/2-\zeta|}{v_s}} \tag{52}$$

At this point we make one final assumption. Since $v=0$, it is necessary to assume a symmetric normal load distribution that will impose symmetry in the friction forces. For simplicity, we choose $f_n=F_n/L=\text{const}$. Recall that

$$\mu_y^{ss}=-\sigma_{0y}z_y^{ss}-\sigma_{2y}v_{ry} \tag{53}$$

Since z_y^{ss} is symmetric with respect to the center of the patch (Fig. 6), and assuming a uniform load distribution, we conclude that the lateral forces cancel each other resulting to $F_y^{ss}=0$. Using (20) we compute

$$\begin{aligned} M_z^{ss} = &-2(\mu_{sy}+\mu_{ky})f_n\left(\frac{v_s}{\dot{\phi}\mu_{ky}}\right)^2\left(1-e^{-\frac{L\dot{\phi}\mu_{ky}}{2v_s}}\right) \\ &+(\mu_{sy}-\mu_{ky})f_n\left(\frac{v_s}{\dot{\phi}\mu_{ky}}\right)Le^{-\frac{L\dot{\phi}\mu_{ky}}{2v_s}} \\ &-\frac{1}{12}\sigma_2\dot{\phi}f_nL^3 \end{aligned} \tag{54}$$

The equation above is what the distributed model predicts in the case where $\omega, v=0$ and $\dot{\phi}=\text{const}$. (i.e., in steady-state). We will compare this with the torsional component of the lumped model (44)-(46) in steady-state. We have

$$\begin{aligned} z_z^{ss} &= \text{sign}(\dot{\phi})\frac{g_z(\dot{\phi})}{\sigma_{0z}} \\ M_{z-tor}^{ss} &= -F_nL\left(\sigma_{0z}z_z^{ss}+\sigma_{2z}\dot{\phi}\right) \end{aligned} \tag{55}$$

For different values of $\dot{\phi}$ we have identified the parameters $\mu_{sz}, \mu_{kz}, \dot{\phi}_s, \sigma_{2z}$ and β by comparing the plots generated by (54) and (55). The parameters identified using the steady states are shown at the following table and the result of the curve fitting is shown in Fig. 6.

Table 3: Identified Parameters

μ_{kz}	μ_{sz}	σ_{2z}	$\dot{\phi}_s$	β
0.0078	0.0975	0	37	1

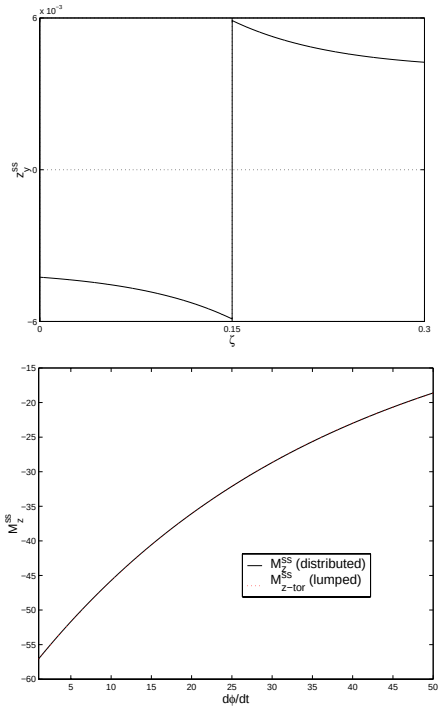

Figure 6: z_y^{ss} distribution and M_{z-tor}^{ss} term fitting

6 Conclusion

An extension of the LuGre dynamic tire friction model from the longitudinal to the combined longitudinal/lateral motion has been presented. Contrary to previous results in the literature, where this extension was performed in an ad hoc manner, directly from the longitudinal LuGre *tire* friction model, here we derive the 2D model, from first principles, by applying the LuGre *point* friction model to the tire/ground interface. The model proposed also captures the anisotropy of the static friction characteristics. In fact, the model agrees with the one presented in [5] for $\mu_{kx} = \mu_{ky}$ and $\mu_{sx} = \mu_{sy}$. Finally, the effects of the wheel rim rotation were taken into account.

7 Acknowledgements

This work was partially supported by CNRS and NSF (award No. INT-9726621/INT-9996096). The work of the first two authors was also supported by the US Army Research Office (contract No. DAAD19-00-1-0473).

References

[1] C. Canudas de Wit and P. Tsiotras, "Dynamic tire friction models for vehicle traction control," in *Proceedings of 38th IEEE Conference on Decision and Control*, (Phoenix, Arizona, USA), pp. 3746–3751, 1999.

[2] J. Deur, "Modeling and analysis of longitudinal tire dynamics based on the LuGre friction model," Tech. Rep., Ford Motor Company, Scientific Research Laboratory MD 1170, Dearborn, MI 48121-2053, USA, 2001.

[3] C. Canudas de Wit, P. Tsiotras, E. Velenis, M. Basset, and G. Gissinger, "Dynamic friction models for road/tire longitudinal interaction," *Vehicle System Dynamics*, (under review).

[4] X. Claeys, C. Canudas de Wit, J. Yi, R. Horowitz, L. Alvarez, and L. Richard, "A new 3d dynamic tire/road friction model for vehicle simulation and control," in *Proceedings of the ASME-IMECE World Conference*, (New York, USA), November 2001.

[5] J. Deur, J. Asgari, and D. Hrovat, "A dynamic tire friction model for combined longitudinal and lateral motion," in *Proceedings of the ASME-IMECE World Conference*, (New York, USA), November 2001.

[6] E. Bakker, L. Nyborg, and H. Pacejka, "Tyre modelling for use in vehicle dynamics studies," *SAE paper # 870421*, 1987.

[7] M. Sorine and J. Szymanski, "A new dynamic multi d.o.f. tire model," in *Transportation Systems 2000*, (Braunschweig, Germany), 2000.

[8] M. Sorine, "Applications of hysteresis models: Contact friction in tires, muscle contraction," in *IEEE CDC 98 Workshop #2*, (Tampa, Florida), 1998.

[9] C. Canudas de Wit, H. Olsson, K. J. Astrom, and P. Lischinsky, "A new model for control of systems with friction," *IEEE Transactions on Automatic Control*, vol. 40, no. 3, pp. 419–425, 1995.